Flexible and Printed Electronics

Methods for short-circuit risk evaluation and reduction in printed electronics based on a filled micro-channel

Flexible and Printed Electronics

PAPER

Methods for short-circuit risk evaluation and reduction in printed electronics based on a filled micro-channel

Shanyou Zhu[1,2], Rui Liu[1,*], Cheng Tang[1,2], Subin Jiang[3], Chao Zeng[3], Ke Shui[2], Jian Lin[2,3,*] and Chang-Qi Ma[2,3,*]

[1] National Demonstration Centre for Experimental Materials Science and Engineering Education, Jiangsu University of Science and Technology, Zhenjiang 212003, People's Republic of China
[2] Printable Electronics Research Centre, Suzhou Institute of Nano-tech and Nano-bionics, Chinese Academy of Sciences, Suzhou Industrial Park, Suzhou, Jiangsu Province 215123, People's Republic of China
[3] Engineering Centre of Precision Printing Manufacturing, Guangdong Institute of Semiconductor Micro-Nano Manufacturing Technology, Kejiao Road No. 1, Shishan Town, 528225 Foshan, People's Republic of China
* Authors to whom any correspondence should be addressed.

E-mail: liurui@just.edu.cn, jlin2010@sinano.ac.cn and cqma2011@sinano.ac.cn

Keywords: micro-channel, short-circuit risk, printed electronics, satellite droplet, sidewall height, contact angle

OPEN ACCESS

RECEIVED
29 September 2024

REVISED
11 February 2025

ACCEPTED FOR PUBLICATION
20 February 2025

PUBLISHED
6 March 2025

Abstract

As one of the key challenges in high-resolution printed electronics, short-circuits are difficult to detect and eliminate in mass production. In this work, high-resolution circuits were fabricated by filling conductive ink into the micro-channels on glass substrates with SU-8 sidewalls. The value of satellite droplet area percentage, which was used as an index for short-circuit risk evaluation, was reduced by improving the contact angle and height of the sidewalls. The sample with a hydrophilic SU-8 sidewall is measured to short-circuit because of the silver ink connecting adjacent printed lines. In contrast, the typical satellite droplet area percentage value of the CF_4 plasma treated sample can be only 0.2% of the untreated one. On the other hand, the sample with the lowest sidewall height of 1.3 μm has the minimum typical satellite droplet area percentage, which is only about 0.64% of the sample with the highest sidewall. Interestingly, the other samples with a variable range of sidewall heights have quite similar silver layer thickness values, while the optimized silver thickness was increased by more than 50% compared to these samples. A multi-channel capacitive-type sensor array was also used to print detect the short-circuit defects efficiently. These results revealed that it is possible to improve the short-circuit risk monitoring and reduction in high-resolution mass printed electronics in the future.

1. Introduction

As a novel technology using conventional printing processes, printed electronics offer advantages including low cost, simplicity, and environmental friendliness [1, 2]. So far a series of functional nanomaterials have been printed as ink to form electronic functional films with specific patterns and structures [3, 4]. The most popular electronics-printing technologies include screen printing, inkjet printing, and doctor blade coating [4], which have been considered as benchmarks and mature technologies for industrialization.

However, the risk of short-circuits is more common in high-resolution printed electronics due to ink flow and printing defects [5], even though the printable conductive materials have been explored widely [6, 7]. Considering that the various methods to prevent them in traditional electronic products [8, 9], the short-circuit risk is the biggest obstacle limiting the industrialization of printed electronics applications. As a result, the printing method has not yet been widely applied in the mass production of electronics, especially with fine patterns less than 50 μm [4]. This challenge will further increase when organic [10] or stretchable [11] integrated circuits are developed in the future.

To prevent short-circuit risks between the adjacent patterns, the printed materials have been controlled by methods including sequential printing and drying [12] or coffee-ring [13]. As a universally applicable method, the surface energy difference [14] was more generally used for restricting ink flow on the substrate. However, the ink stay on the hydrophobic

surface can split into satellite droplets [15], which introduce short-circuit risks between adjacent printed lines or patterns. Micromolded hydrophobic separators with certain height have also been reported to define the ink flow for a short channel of source/drain electrodes [16], which can restrict the ink flow by better utilizing the gravitational effect to pull the ink downhill to the conductive pattern region. On the other hand, the adaptive printed circuits with high-resolution thin conducive lines require micro-channel structures to better control the ink flow, which is much more complex than source/drain electrode fabrication using a dewetting separator. Meanwhile, micro-channel sidewalls with lower surface energy have been reported for laminar drag reduction [17] and dried ink profile improvement [18].

However, it has also been reported that densely arrayed dewetting microstructures may allow water to stand away from the substrate because of the Cassie state [19, 20]. To avoid large contact angles, the micro-channels were usually plasma treated to improve their hydrophilic properties for filling ink better [21] before fabricating conductive patterns. It was also reported that the Cassie state turns to complete wetting quickly when the water-air interface touches the bottom of the micro-channels [20]. It can therefore be hypothesized that there may be a critical value of the sidewall height for ink filling in micro-channels. In other words, the contact angle and height of the micro-channel sidewall probably play key roles for reducing short-circuit risk in the conductive patterning method based on micro-channels.

In this paper, high-resolution circuits were fabricated by blade coating silver (Ag) conductive ink into the micro-channels on glass substrates. Ag ink was filled on the uncovered glass substrate between the sidewalls to form the conductive thin lines. Dried ink droplets on the sidewall surface between conductive lines, which may lead to short-circuits, were named as satellite droplets in this work. The sidewalls designed with proper contact angles and varying heights were fabricated using a spin-coated SU-8 photoresist. The samples' contact angles were improved using CF_4 gas plasma treatment. The different sidewall heights were obtained by changing the value of SU-8 layer thickness. The value of satellite droplet area percentage, which was used as an index of short-circuit risk evaluation, was reduced by improving the sidewall contact angles and heights. A multi-channel capacitive-type sensor array was also used to detect the short-circuit defects efficiently.

2. Materials and methods

2.1. Materials

The Ag conductive ink (Ag particles with 30–50 nm diameter, 35–40 wt%) was purchased from BroadTeko. Propylene glycol monomethyl ether acetate (PGMEA) was provided by Adamas-beta. SU-8 3010 negative epoxy photoresists were purchased from Microchem. All of the materials were used without further purification.

2.2. Preparation of conductive patterns

SU-8 micro-channel fabrication: The glass substrate was cleaned using detergent, anhydrous ethanol, and deionized water sequentially. It is then treated with oxygen plasma for 3 min to enhance the adhesion of the glass substrate surface. The SU-8 negative epoxy photoresist, which was diluted using PGMEA with ratios of 1:1, 2:1, 3:1, 4:1, and 1:0 respectively, was spin-coated (6000 rpm) on the glass substrate as shown in figure 1(a). The photolithography was then performed, as shown in figure 1(b), which contains a series of steps as follows. The sample was soft baked using a 100 °C hot plate before UV exposure. The sample was then successively placed in an SU-8 photoresist developer, isopropanol, and deionized water for developing, rinsing, and washing, respectively, followed by drying with a nitrogen gun. The thickness of the spin-coated SU-8 layer, which was varied because of the different diluted ratios, was considered as the sidewall height of the micro-channel. As an optional process, the samples can be CF_4 gas plasma treated for different contact angles, as shown in figure 1(c).

Ag ink filled micro-channel fabrication: The water-based Ag ink was filled into the micro-channels composed of SU-8 sidewalls and uncovered glass substrate using a ZAA2300 Automatic Film Applicator with a speed of 1 mm s^{-1}. Then, the filled sample was sintered on a hot plate at 250 °C. Finally, a sample with high-resolution circuits was obtained. All of the steps are shown in figures 1(d)–(f).

2.3. Characterization and measurement

The samples with dried ink were observed using optical microscopy, with the satellite droplets detected and analyzed by ImageJ. X-ray photoelectron spectroscopy (XPS) measurements were recorded using the Kratos Asxis Ultra DLD. Contact angle of the surface was measured using SinDin Precision SDC-200 S. The surface energy was calculated based on the measured contact angles of water and diiodomethane. Considering that the surface energy of the photoresist material is mainly determined by the surface topography and surface chemistry, the measured contact angle and surface energy of the sidewall surface should have the same value as the horizontal surface area of the same sample. As a result, the measured contact angles on the horizontal SU-8 surface area were used instead of the contact angles of the sidewall surfaces. A 160 × 160 multi-channel readout circuit (GP Nano, GP-FMA-05) for a capacitive-type sensor array was used to detect the short-circuit defects of the printed samples.

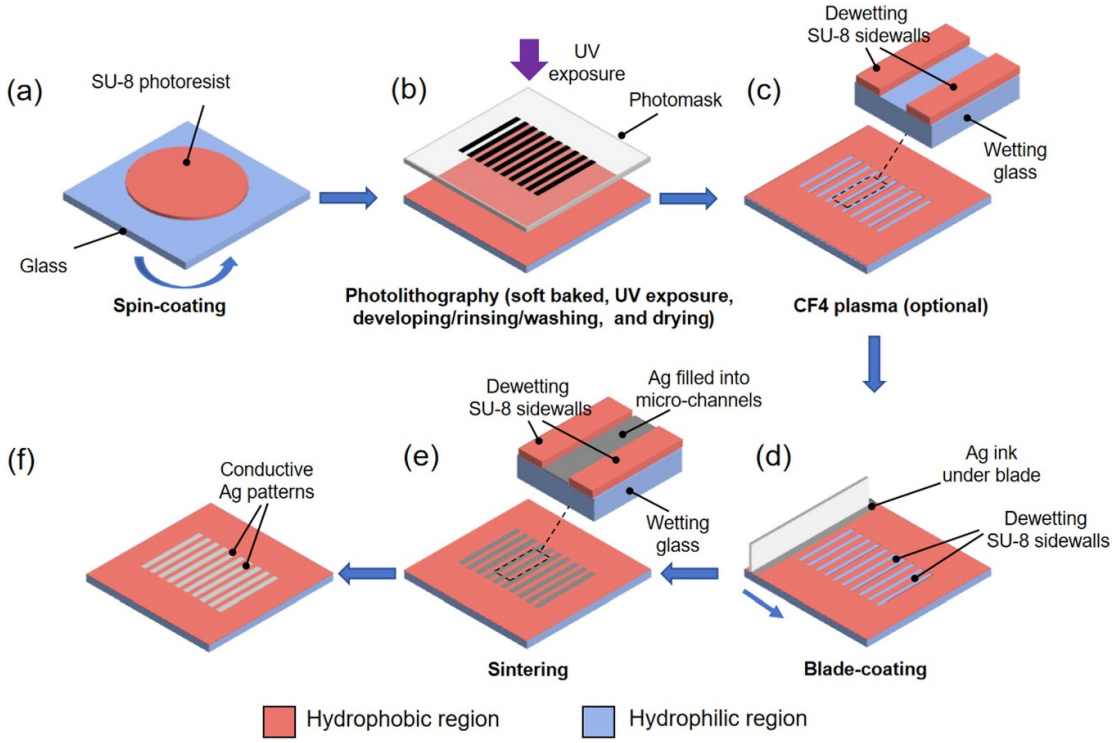

Figure 1. Steps of pattern fabrication and printing: (a)–(b) schematic diagram of the micro-channels fabrication process with different surface energies. (c)–(f) Schematic diagram of ink blade coating and sintering.

3. Results

3.1. The role of sidewall contact angles

By means of blade-coating, the ink is filled on the uncovered glass substrate between the SU-8 sidewalls and then dried as a thin solid Ag layer. To investigate the role of the contact angles intuitively, samples with SU-8 sidewalls are ultraviolet-ozone (UVO) treated before the Ag ink coating to make the contact angles similar between the sidewalls and the uncovered glass substrate surface. The typical water contact angle of the SU-8 surface was decreased from 72.831° to 10.307° after UVO treatment, as shown in figures 2(a)–(c) respectively. However, the UVO treated SU-8 surface is spanned by the dried Ag ink very seriously after ink filling and baking, as shown in figure 2(a). Figure 2(b) also confirms the short-circuit behavior of the conductive micro-channels, which are in full accord with the spanned ink observed by optical microscopy. These results show that it is very important for short-circuit reducing to avoid wetting of the sidewall surfaces.

Furthermore, the distribution density of satellite droplets that remain on the sidewalls also proved to be an index for evaluating the short-circuit risk of the printed samples because of this result. In contrast, samples without UVO treatment have quite clean sidewall surfaces and seldom have satellite droplets. The images of the measured contact angles and optical microscopy are shown in figure 2(c).

It is worth mentioning that the water contact angle decreases from 44.211° to 3.398° after the UVO treatment, which means increased capillary force which can promote attractive interactions between ink and glass surface [14]. The gravitational effect can also pull ink downhill because of the height difference between the sidewall and glass. However, the sidewall surface with UVO treatment (figure 2(a)) still has much more dried ink stay than the sample in figure 2(c). The most reasonable explanation for this result is that the repellency of the micro-channel sidewall surface plays a more important role in reducing the spanned ink than the hydrophilic property of the glass substrate surface.

It was reported that polymer surface can turn hydrophobic due to fluorination after CF_4 gas plasma treatment [22], while the adjacent glass surface remains hydrophilic [23]. These reports indicate that a short-time CF_4 gas plasma treatment can be used to modify the contact angle of the sidewall surface. To find out if this method is effective enough, the samples are CF_4 plasma treated for 0 s, 1 s, 2 s, 4 s, and 8 s. The satellite droplets stayed on the sidewall surface and were detected and analyzed by ImageJ. Table 1 shows that the samples treated for different times have typical satellite droplet area percentages of 0.0461, 0.0018, 0.0001, 0.0099, and 0.0115, which were analyzed from the images in figure 3(a). It was found that the sample with 2 s CF_4 plasma treatment has the lowest satellite droplet area percentage, which

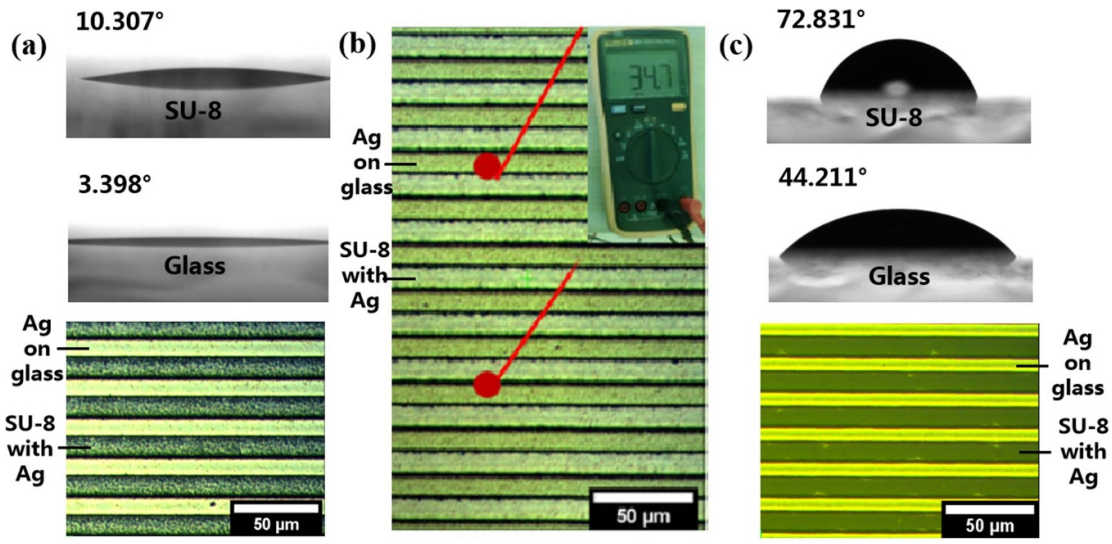

Figure 2. (a) The measured contact angles and optical microscopic image of the sample with UVO treatment. (b) The optical microscopic image of a short-circuit detected sample, with the inset showing the measured resistance value using a multimeter. (c) The measured contact angles and optical microscopic image of the sample without UVO treatment.

Table 1. Data table of surface satellite droplets with the CF_4 plasma treatment for different seconds.

Treatment time (s)	Satellite droplet area (px^2)	Area percentage	Measured typical contact angles
0	30 306	0.0461	62.49°
1	1189	0.0018	71.56°
2	45	0.0001	74.93°
4	6559	0.0099	65.58°
8	7618	0.0115	59.12°

is only about 0.2% of the value measured from the untreated sample.

The contact angles on the SU-8 surfaces with the CF_4 plasma treated for different times were used to explain the satellite droplet area percentage change trends. For more accurate characterization, the Ag ink contact angle was used instead of the water contact angle. Figure 3(b) shows the SU-8 surface CF_4 plasma treated for 2 s has the largest typical contact angle of 74.93°, while the typical values of other SU-8 surfaces are 62.49°, 71.56°, 65.58°, and 59.12° for 0, 1, 4, and 8 s, respectively. This shows a consistent trend that sidewall surfaces with larger water contact angles have lower satellite droplet area percentage. The surface energies were also calculated using the measured contact angles of water and diiodomethane, of which the comparison is shown in figure 3(c).

To understand the relationship between CF_4 gas plasma treatment and contact angle changes, XPS was used to observe the chemical bonds on the SU-8 surface. Figure 3(d) shows the measured C1s spectra, which confirms that newly formed C–F, C–F_2 and C–F_3 bonds were induced in the SU-8 surface after the CF_4 plasma treatment. The decrease in the intensities of the C–O and C–C peaks in figure 3(d) could also be attributed to the breaking of these bonds during the fluorination process in the CF_4 treatment process. These results confirm that the SU-8 surface became hydrophobic after it was fluorinated with the increased bond numbers of C–F, C–F_2 and C–F_3, which is similar to the reported work [24]. The methodology of improving contact angles by bonds changing has been widely applied in various materials [25, 26] and is considered to be a mature method.

In brief, it can be found that the observed satellite droplet area percentages were in the negative direction significantly with the water contact angles of SU-8 sidewalls. This means the sidewall surface with larger water contact angle can reduce short-circuit risk by repelling ink away, which is similar to the reported work [16]. Considering the above-mentioned UVO treated sample also shows that the ink repellency of the micro-channel sidewall surface plays a more important role in preventing the short-circuit, this conclusion demonstrates adequate repeatability.

3.2. The role of sidewall height

Besides the above-mentioned factor of contact angle differences, the influence between the sidewall height and its satellite droplet area ratios was also studied. Furthermore, to find out the satellite droplet area differences only because of the sidewall height variation, the samples without CF_4 plasma treatment were used for the comparison. Figure 4(a) shows that the sample with 1.3 μm sidewalls has the lowest typical satellite droplet area and area ratios, while the sample with the largest sidewall height of 8.1 μm has the most serious satellite droplets. The results of satellite droplet areas and area ratios on the sidewall surface were also

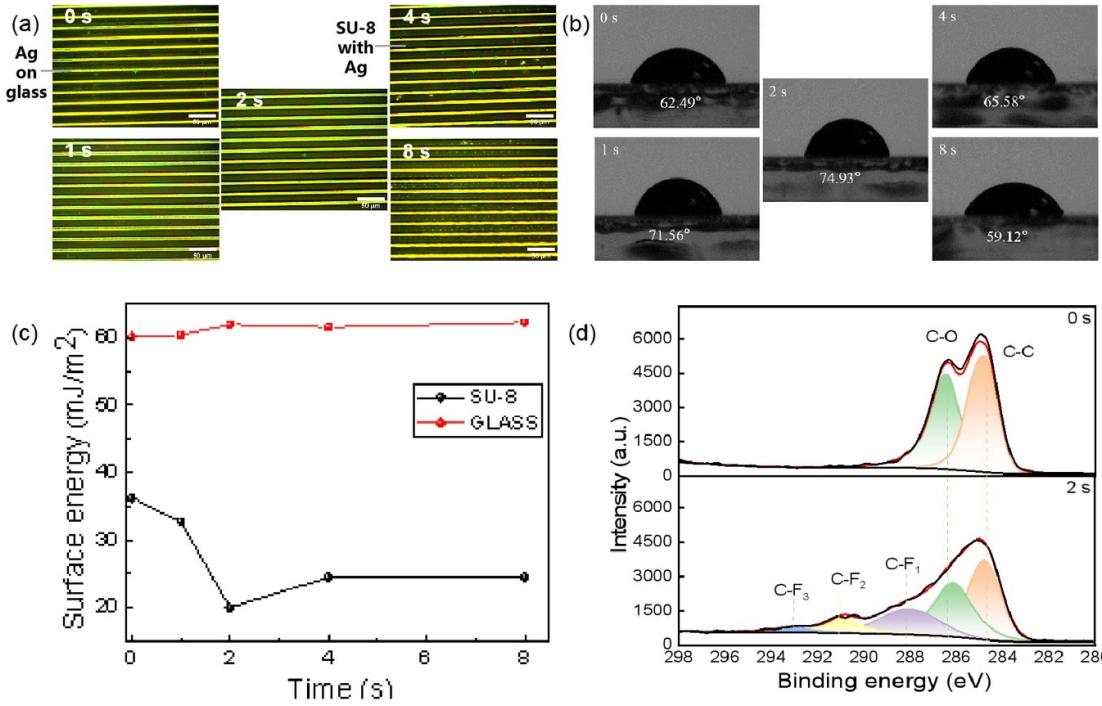

Figure 3. (a) Comparison of the satellite droplets on the sidewall surface of Ag filled samples with the CF_4 plasma treatment for different times. (b) Comparison of the Ag ink contact angles on horizontal SU-8 surfaces with CF_4 plasma treatment for different times. (c) Comparison of the calculated surface energies with CF_4 plasma treatment for different times. (d) Comparison of C1s spectra of the SU-8 surface XPS with CF_4 plasma treatment for 0 and 2 s.

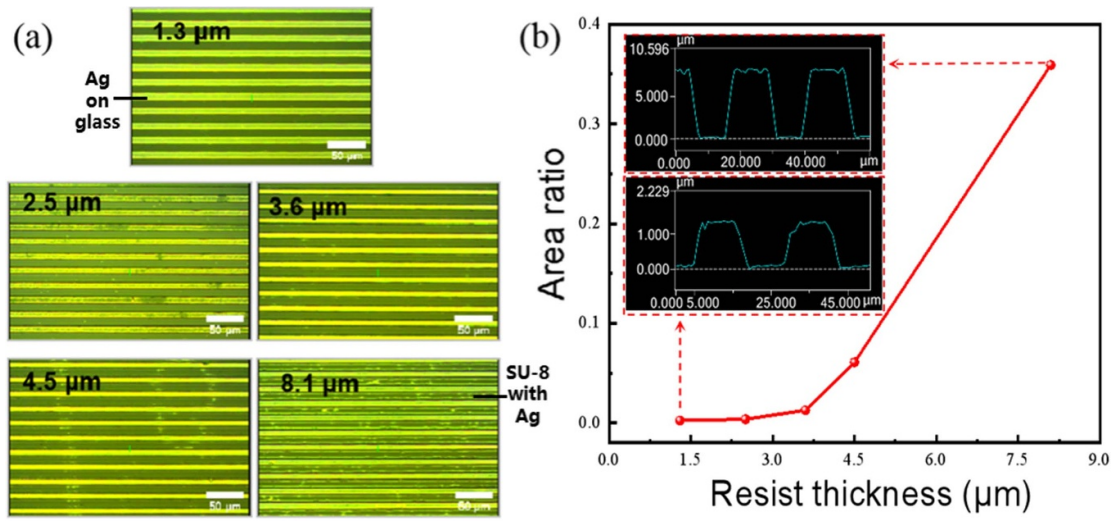

Figure 4. (a) Comparison of the satellite droplets on samples with different sidewall heights observed by optical microscope. (b) Comparison of the area ratios on the surfaces of Ag filled samples with different sidewall heights. Inset is the profiles of the micro-channel samples with different sidewall heights.

analyzed and obtained in table 2. It is shown that the samples with 1.3 μm, 2.5 μm, 3.6 μm, 4.5 μm and 8.1 μm have typical satellite droplet area percentages of 0.0023, 0.0037, 0.0127, 0.0608, and 0.3591, respectively.

On the other hand, the typical thickness of the filled dried Ag layers with different sidewall heights was also studied using the cross section SEM images. The sample with the lowest sidewall (1.3 μm) was found to have the thickest filled Ag of 0.213 μm typically. The samples with other sidewall heights had quite similar thickness ranges (0.108–0.139 μm) of the dried Ag layers, which is shown in figure 5(b).

To interpret the interesting role of sidewall height, a hypothesis model was put forward as shown in figure 5(c). The blade coated Ag ink stays only at the top of the micro-channels as a meniscus because of the Cassie state, which means the ink meniscus

Table 2. Satellite droplet areas and area ratios on the sidewall surface of Ag filled samples with different sidewall heights.

Sidewall height (μm)	Satellite droplet Area (px^2)	Area ratio
1.3	371	0.0023
2.5	598	0.0037
3.6	2041	0.0127
4.5	9759	0.0608
8.1	57 592	0.3591

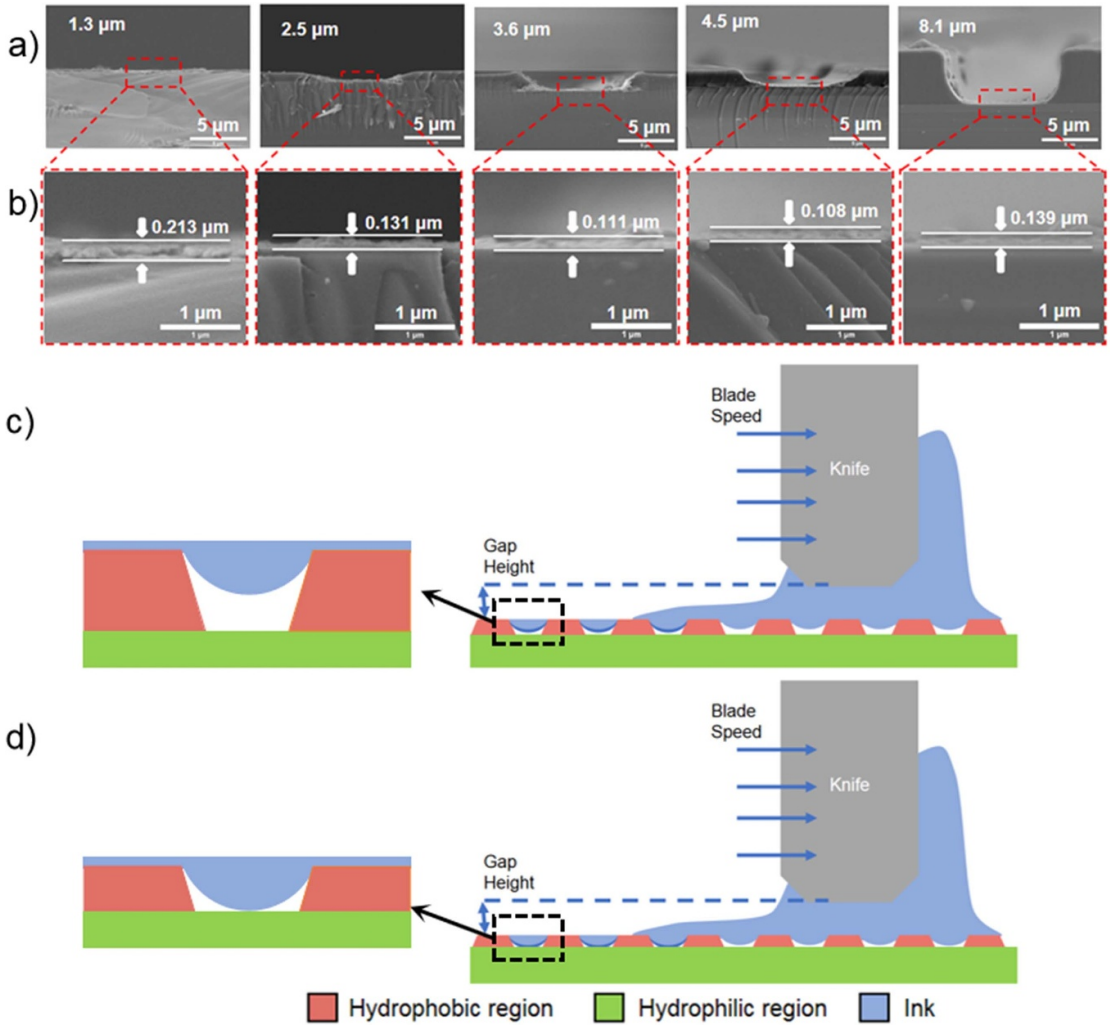

Figure 5. (a) and (b) The cross section SEM images of the Ag filled samples with different sidewall heights. (c) Schematic diagram of the liquid flow during the ink filling process with larger sidewall height. (d) Schematic diagram of the liquid flow during the ink filling process with low sidewall height.

cannot touch the wetting glass surface if the sidewall height is too large, as shown in figure 5(c). Considering that the mechanical balance depends on the contact angle of the ink on the sidewall surface and the width of the micro-channel, the ink stay upon the micro-channels with different sidewall heights should be the same. In fact, the samples with the sidewall height range of 2.5–8.1 μm indeed have quite similar values of dried Ag layer thickness.

In contrast, the dried Ag layer thickness of the sample with the lowest sidewall was increased by more than 50% compared to other samples with larger sidewall heights. This is because the ink-air interface can touch the wetting glass surface when the sidewall height is low enough, as shown in figure 5(d). The surface tension between the ink and the glass surface can lead to more ink stay on the wetting glass surface between the sidewalls. On the other hand, the ink on samples with large sidewall heights can also move downhill to the glass surface because of other forces such as gravity (not shown in figure 5(c)), though the ink volume was obviously reduced. The rest of the Ag ink stays, splits, and dries on the SU-8 surface, leading to the increased satellite droplet areas and area ratios.

Considering the role of sidewall contact angles discussed above, the general conclusion is that higher

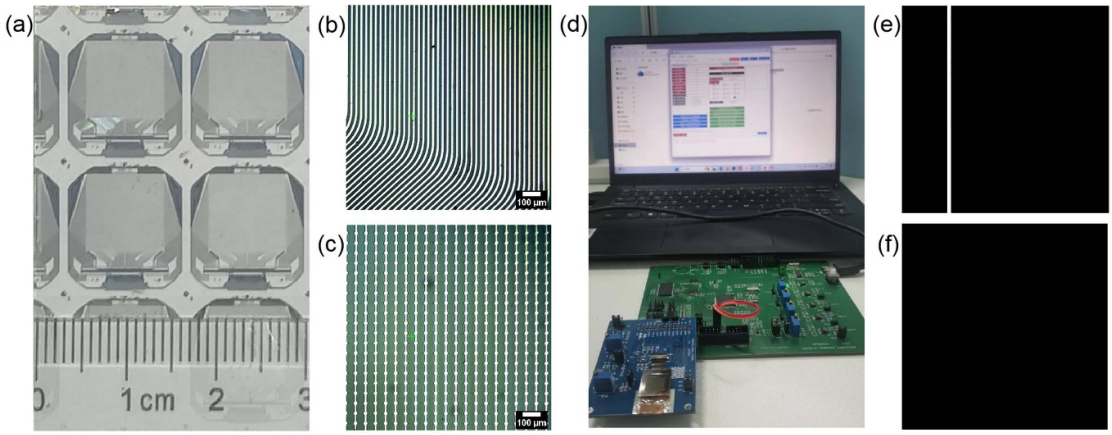

Figure 6. (a) The overall appearance of the 160 × 160 multi-channel capacitive-type sensor arrays. (b) Part of the printed signal lines with 10 μm width and distance. (c) Part of the electrode pixels at an array period of 50 μm. (d) The self-made equipment for detecting the short-circuit defects. (e) An output BMP image with vertical short-circuit defects detected. (f) An output BMP image without any short-circuit defect detected.

contact angle and lower sidewall height can reduce the short circuit risk in the printed electronics based on filled micro-channel significantly. The role of gravitational effects, such as pulling the ink downhill to the conductive pattern region, is weaker than the capillary force which repels the ink away from the micro-channel sidewall surfaces with higher contact angles. On the other hand, larger sidewall heights can also make the ink filling into the micro-channels more difficult. Then, more printed ink remains between the conductive lines as satellite droplets, which can increase the risk of short circuits.

3.3. Capacitor array for short-circuit detection

To meet the challenge of accurately detecting short-circuit defects efficiently and conveniently, a multi-channel readout circuit for a capacitive-type touch-screen panel was used in this work. A capacitive-type sensor array with 160 × 160 multi-channel readout circuit, which has the pixels at an array period of 50 μm, is fabricated using the Ag ink filled method in this work. The overall appearance, part of the signal lines with 10 μm width/distance, and part of electrode pixels are shown in figures 6(a)–(c), respectively. Such samples were then read using self-made equipment, which can check if there is any short-circuit defect in the 25 600 pixels by reading the signals within a period of no more than 200 ms (figure 6(d)). The output BMP images with or without short-circuit defects detected can be found in figures 6(e) and (f). The white dots in the image, which means the pixels at corresponding positions output a much stronger signal, can be used to detect that there are short-circuit defects present.

The strong capacitance change due to short-circuits in the conductive lines or capacitive sensor electrodes can be used to explain the above-mentioned stronger signal (white dots in the image). The varied mutual capacitances are monitored very sensitively by the signals transferred from the transmitter (Tx) to the receiver (Rx) via the electrodes in this kind of multi-channel capacitive sensor array [27]. As a result, the more significant capacitance difference due to short-circuits can be detected very easily using this kind of multi-channel readout circuit for capacitive-type touch-screen panels.

4. Conclusions

In summary, high-resolution circuits were fabricated by blade coating conductive ink into the micro-channels with a glass substrate. The contact angle and height of the sidewall were confirmed to play key roles in reducing the risks of short-circuits. The sample with hydrophilic SU-8 sidewall surface is spanned by the Ag ink very seriously, with its short-circuit behavior confirmed by electrical measurement. In contrast, the typical satellite droplet area percentage value of the sample with CF_4 plasma treated SU-8 sidewalls can be as low as 0.2% of the value of the untreated sample. Additionally, the sample with the lowest sidewall height of 1.3 μm has the minimum typical satellite droplet area percentage of 0.0023, which is only about 0.64% of the largest value of 0.3591 from the sample with the highest 8.1 μm sidewall. Furthermore, the samples with the sidewall height range of 2.5–8.1 μm have quite similar values of Ag layer thickness, while the Ag thickness of the sample with the lowest sidewall was increased by more than 50% compared to other samples. Therefore, our work identifies that both the higher surface contact angle and lower height of the sidewall can reduce the short circuit risk.

To detect short-circuit defects efficiently, a capacitive-type sensor array with 50 μm array period and 160 × 160 multi-channel readout circuit was fabricated, in which the detected short-circuit defects

of the 25 600-pixels can be found from an output BMP image. These studies open up the possibility for continuing research on short-circuit risk monitoring and reduction for high-resolution mass printed electronics in the future.

Data availability statement

All data that support the findings of this study are included within the article (and any supplementary files).

Acknowledgment

This work was supported by Guangdong Basic and Applied Basic Research Foundation (Grant No. 2020B1515120059).

ORCID iDs

Jian Lin https://orcid.org/0000-0002-3037-7023
Chang-Qi Ma https://orcid.org/0000-0002-9293-5027

References

[1] Khan S, Lorenzelli L and Dahiya R S 2015 Technologies for printing sensors and electronics over large flexible substrates: a review *IEEE Sens. J.* **15** 3164–85
[2] Khan Y, Thielens A, Muin S, Ting J, Baumbauer C and Arias A C 2020 A new frontier of printed electronics: flexible hybrid electronics *Adv. Mater.* **32** 1905279
[3] Chen S and Liu J 2022 Liquid metal printed electronics towards ubiquitous electrical engineering *Jpn. J. Appl. Phys.* **61** SE0801
[4] Martins P, Pereira N, Lima A C, Garcia A, Mendes-Filipe C, Policia R, Correia V and Lanceros-Mendez S 2023 Advances in printing and electronics: from engagement to commitment *Adv. Funct. Mater.* **33** 2213744
[5] Jo M, Lee J, Kim S, Cho G, Lee T-M and Lee C 2021 Resistance control of an additively manufactured conductive layer in roll-to-roll gravure printing systems *Int. J. Precis. Eng. Manuf.—Green Technol.* **8** 817–28
[6] Lu X, Zhang Y and Zheng Z 2021 Metal-based flexible transparent electrodes: challenges and recent advances *Adv. Electron. Mater.* **7** 2001121
[7] Slavin Y N, Asnis J, Häfeli U O and Bach H 2017 Metal nanoparticles: understanding the mechanisms behind antibacterial activity *J. Nanobiotechnol.* **15** 65
[8] Kim T, Yun T H, Yim C and Kim J 2023 Fabrication of short circuit-preventing electrodes with a self-assembled monolayer on flashlight-sintered porous copper nanofilms *Int. J. Precis. Eng. Manuf.-Smart Tech.* **24** 43–52
[9] Lee J-A, Sim D H and Lee B K 2024 Short-circuit protection for SiC MOSFET based on PCB-type Rogowski current sensor: design guidelines, practical solutions, and performance validation *IEEE Trans. Power Electron.* **39** 3580–9
[10] Chen Q *et al* 2024 Contact engineering for organic CMOS circuits *J. Phys. Mater.* **7** 012002
[11] Zhong D *et al* 2024 High-speed and large-scale intrinsically stretchable integrated circuits *Nature* **627** 313–20
[12] Naderi P, Sheuten B R, Amirfazli A and Grau G 2023 Inkjet printing on hydrophobic surfaces: Controlled pattern formation using sequential drying *J. Chem. Phys.* **159** 024712
[13] Li Y, Lan L, Xiao P, Sun S, Lin Z, Song W, Song E, Gao P, Wu W and Peng J 2016 Coffee-ring defined short channels for inkjet-printed metal oxide thin-film transistors *ACS Appl. Mater. Interfaces* **8** 19643–8
[14] Shui K *et al* 2023 UV-converted heterogeneous wettability surface for the realization of printed micro-scale conductive circuits *Flex. Print. Electron.* **8** 035019
[15] Zou L, Wang H, Zhu X, Ding Y, Chen R and Liao Q 2018 Droplet splitting on chemically striped surface *Colloids Surf. A* **537** 139–48
[16] Jeong J, Kim M, Lee S-H, Kim D, Kim T and Hong Y 2011 Self-defined short channel formation with micromolded separator and inkjet-printed source/drain electrodes in OTFTs *IEEE Electron Device Lett.* **32** 1758–60
[17] Ou J, Perot B and Rothstein J P 2004 Laminar drag reduction in microchannels using ultrahydrophobic surfaces *Phys. Fluids* **16** 4635–43
[18] Tang C, Liu R, Zhu S, Jiang S, Shui K, Lin J and Ma C-Q 2024 Profile improvement of blade coated circuits by the capillary force originating from the hydrophobic sidewalls *Flex. Print. Electron.* **9** 035009
[19] Ding Y, Jia L, Peng Q and Guo J 2020 Critical sliding angle of water droplet on parallel hydrophobic grooved surface *Colloids Surf. A* **585** 124083
[20] Papadopoulos P, Mammen L, Deng X, Vollmer D and Butt H-J 2013 How superhydrophobicity breaks down *Proc. Natl Acad. Sci.* **110** 3254–8
[21] Wang Z, Yi P, Peng L, Lai X and Ni J 2017 Continuous fabrication of highly conductive and transparent Ag mesh electrodes for flexible electronics *IEEE Trans. Nanotechnol.* **16** 687–94
[22] Oberlintner A, Shvalya V, Vasudevan A, Vengust D, Likozar B, Cvelbar U and Novak U 2022 Hydrophilic to hydrophobic: ultrafast conversion of cellulose nanofibrils by cold plasma fluorination *Appl. Surf. Sci.* **581** 152276
[23] Lee S Y, Sakong C, Choi S-H, Ju B-K and Cho K H 2023 Controlling the surface modification by CF4 plasma treatment for inkjet printed color conversion layer with InP-based QDs Ink *Adv. Mater. Interfaces* **10** 2201851
[24] Babu S, Dousti B, Lee G S and Lee J-B 2021 Conversion of polymer surfaces into nonwetting substrates for liquid metal applications *Langmuir* **37** 8139–47
[25] Sprang N, Theirich D and Engemann J 1998 Surface modification of fluoropolymers by microwave plasmas: FTIR investigations *Surf. Coat. Technol.* **98** 865–71
[26] Naderi P and Grau G 2022 Organic thin-film transistors with inkjet-printed electrodes on hydrophobic Teflon-AF gate dielectric with reversible surface properties *Org. Electron.* **108** 106612
[27] Park S-H, Kim H-S, Bang J-S, Cho G-H and Cho G-H 2017 A 0.26-nJ/node, 400-kHz Tx driving, filtered fully differential readout IC with parasitic RC time delay reduction technique for 65-in 169×97 capacitive-type touch screen panel *IEEE J. Solid-State Circuits* **52** 528–42